Change in drag, apparent slip and optimum air layer thickness for laminar flow over an idealised superhydrophobic surface

A. BUSSE[1], N. D. SANDHAM[1], G. MCHALE[2] AND M. I. NEWTON[3]

[1]Faculty of Engineering and the Environment, University of Southampton, Highfield, Southampton, SO17 1BJ, United Kingdom

[2] Faculty of Engineering and Environment, Northumbria University, Newcastle upon Tyne NE1 8ST, United Kingdom

[3] School of Science and Technology, Nottingham Trent University, Clifton Lane, Nottingham NG11 8NS, United Kingdom

(Received 12 July 2013)

Analytic results are derived for the apparent slip length, the change in drag and the optimum air layer thickness of laminar channel and pipe flow over an idealised superhydrophobic surface, i.e. a gas layer of constant thickness retained on a wall. For a simple Couette flow the gas layer always has a drag reducing effect, and the apparent slip length is positive, assuming that there is a favourable viscosity contrast between liquid and gas. In pressure driven pipe and channel flow blockage limits the drag reduction caused by the lubricating effects of the gas layer; thus an optimum gas layer thickness can be derived. The values for the change in drag and the apparent slip length are strongly affected by the assumptions made for the flow in the gas phase. The standard assumptions of a constant shear rate in the gas layer or an equal pressure gradient in the gas layer and liquid layer give considerably higher values for the drag reduction and the apparent slip length than an alternative assumption of a vanishing mass flow rate in the gas layer. Similarly, a minimum viscosity contrast of four must be exceeded to achieve drag reduction under the zero mass flow rate assumption whereas the drag can be reduced for a viscosity contrast greater than unity under the conventional assumptions. Thus, traditional formulae from lubrication theory lead to an overestimation of the optimum slip length and drag reduction when applied to superhydrophobic surfaces, where the gas is trapped.

1. Introduction

Over the last decade interest in the potential application of superhydrophobic surfaces for drag reduction has grown (Neto *et al.* 2005; Quéré 2008; Voronov *et al.* 2008; Vinogradova & Dubov 2012). Superhydrophobic surfaces are structured surfaces with micro- or nano-scale roughness that have a hydrophobic surface chemistry (McHale *et al.* 2010). The combination of hydrophobicity and structuring makes it possible to retain air due to surface tension on the surface when it is immersed in water. Due to the lower dynamic viscosity of air compared to water the trapped air layer on a superhydrophobic surface has a lubricating effect on the flow over it. Drag reducing properties of superhydrophobic surfaces have been observed experimentally in microfluidic devices (Choi *et al.* 2003; Ou *et al.* 2004; Ou & Rothstein 2005; Joseph *et al.* 2006; Govardhan *et al.* 2009; Tsai *et al.* 2009; Daniello *et al.* 2009; Rothstein 2010) and for coated objects, such as hydrofoils (Gotge *et al.* 2005), settling spheres (McHale *et al.* 2009) and cylinders

(Muralidhar *et al.* 2011), covering flow regimes from laminar to turbulent. In a stable configuration, i.e. when the air layer has a constant thickness and is not depleted, the air on a superhydrophobic surface is trapped. This means that there is no net mass flow rate within the air layer irrespective of the water flow past the superhydrophobic surface. In this respect superhydrophobic surfaces differ from other drag reduction mechanisms involving air such as the injection of air upstream of an object where a finite mass flow rate of air has to be maintained (see e.g. Elbing *et al.* 2008). Current research efforts focus on the development of improved superhydrophobic surfaces and on their application on macroscopic scales (Greidanus *et al.* 2011; Gruncell *et al.* 2012*b*), e.g. to the coating of watercraft and the lining of pipes. Elboth *et al.* (2012) recently demonstrated that superhydrophobic coatings can reduce drag on towed streamer cables.

Besides superhydrophobic surfaces, superoleophobic (Tuteja *et al.* 2007; Bhushan 2011) and omniphobic (Tuteja *et al.* 2008; Wong *et al.* 2011) surfaces are also of interest. They are similar to superhydrophobic surfaces in their basic configuration, the main differences being the different surface chemistry, specific shape of micro- or nano-topography, and sometimes the lubricating medium. It is therefore important to study the general dependence of the drag reduction on the viscosity contrast, and not to focus solely on the air-water problem.

Another way of covering a surface immersed in a liquid with a gas layer is to exploit the Leidenfrost effect (Leidenfrost 1966). In a terminal velocity experiment, Vakareslki *et al.* (2011) achieved a perfect enrobing layer of vapour around a heated metal sphere and demonstrated that the terminal velocity could be more than doubled compared to having a direct contact between the metal sphere and the surrounding liquid.

A related problem is the transport of heavy oil in pipes. Here, under certain conditions a perfect core annular flow (PCAF) can be achieved, where the flow of the heavy oil is lubricated by a layer of water on the pipe walls (Joseph *et al.* 1997). Core annular flows can lead to a large decrease of the pressure drop along the pipe, making them of high practical importance (Ghosh *et al.* 2009). The layered flow of oil over water bears a strong resemblance to the flow of water over superhydrophobic surface. However, unlike the air on a superhydrophobic surface, the water in a core annular flow is not trapped. In the case of stratified flows the lubrication of an oil flow by pockets of water has been proposed by *Looman* (Looman 1916; Joseph *et al.* 1997). This bears a closer resemblance to superhydrophobic surfaces since in this case the lubricating medium (here water) is trapped in the pockets.

The aim of this paper is to give upper limits for the drag reduction and the equivalent slip length by investigating laminar flow over a highly idealised superhydrophobic surface. The assumption that the gas on a superhydrophobic surface is trapped, i.e. zero net mass flow downstream, leads to different results for change in drag, the optimum air layer thickness and apparent slip length compared to previous approaches (Than *et al.* 1987; Joseph *et al.* 1984; Vinogradova 1999) where a finite mass flow rate is allowed in the air layer.

2. Basic assumptions

A superhydrophobic surface may be modelled as a continuous air layer of constant thickness δ superimposed on a wall (see figure 1). In the following analysis the supporting structure of a superhydrophobic surface is neglected; only its beneficial effects are kept, i.e. retaining an air layer at the surface which is undeformable, and thus suppressing instabilities at the air-water interface. The potentially drag-increasing properties of the

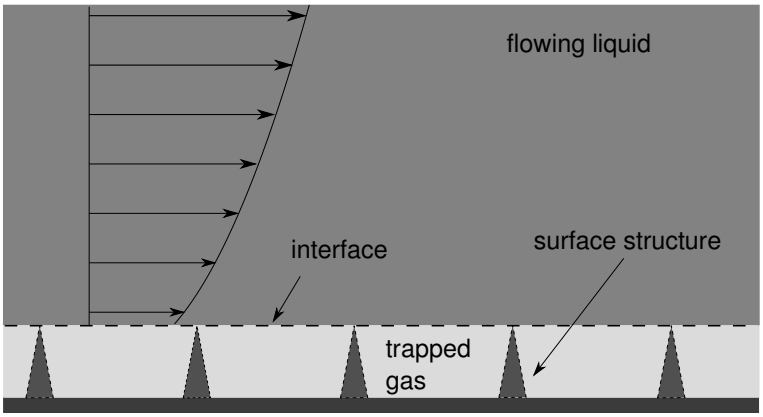

FIGURE 1. Illustration of an idealised superhydrophobic surface.

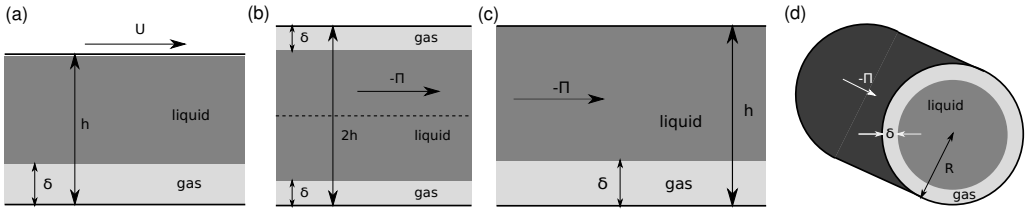

FIGURE 2. Basic flow geometries: (a) Couette flow, (b) symmetric pressure driven channel flow, (c) one-sided pressure driven channel flow, (d) pipe flow.

surface structure due to its roughness are neglected. By neglecting all potentially adverse effects this acts as a model for an 'optimal' superhydrophobic surface.

While the present investigation is mainly aimed at superhydrophobic surfaces, similar problems occur in other contexts as discussed in section 1. Therefore, the general problem of the laminar flow of two immiscible fluids is investigated. The first fluid flows over an infinite layer of constant thickness of the second fluid, which has a lower dynamic viscosity and acts as a lubricant for the flow of the first fluid. In the following, the first fluid will be called 'liquid'. The second fluid will be referred to as 'gas'. The names 'liquid' and 'gas' are adapted only for ease of nomenclature. The second fluid need not be a gas, in the case of the oil-water problem both the first and the second fluid would be liquids.

Four different basic flow configurations, illustrated in figure 2, will be studied:

(a) Couette flow with the lower wall covered by a gas layer,

(b) pressure driven channel flow with both walls covered by gas layers of equal thickness,

(c) pressure driven channel flow with only one wall covered by a gas layer, and

(d) pressure driven pipe flow with the pipe wall covered by a gas layer.

The effects of gravity are neglected, therefore it is arbitrary whether the upper or lower wall is covered by a gas layer in configurations (a) and (c).

We assume a stationary laminar flow, i.e. the flow has only a streamwise velocity component u which depends on the wall-normal coordinate (z or r) only and has no time dependence. The Navier-Stokes equations reduce then to (see e.g. Landau & Lifshitz 1959)

$$\mu \frac{\mathrm{d}^2}{\mathrm{d}z^2} u(z) = \begin{cases} 0 & \text{for the Couette flow case,} \\ \Pi & \text{for the channel flow cases,} \end{cases} \tag{2.1}$$

and to

$$\mu \frac{1}{r}\frac{\mathrm{d}}{\mathrm{d}r} r \frac{\mathrm{d}}{\mathrm{d}r} u(r) = \Pi \quad \text{for the pipe flow case,} \tag{2.2}$$

where Π is the mean streamwise pressure gradient, and μ is the dynamic viscosity. Standard no-slip boundary conditions are applied at the walls. In the pressure driven channel flow cases the walls are assumed to be stationary. In the Couette flow case the lower wall is at rest and the upper wall moves at a constant speed U_0.

At the interface between the liquid and the gas the velocity and the viscous stresses must be continuous (Sadhal *et al.* 1996), giving the following (internal) boundary conditions at the interface (abbreviated by I):

$$u_G|_I = u_L|_I \tag{2.3}$$

and

$$\mu_G \frac{\mathrm{d}}{\mathrm{d}z} u_G(z)\bigg|_I = \mu_L \frac{\mathrm{d}}{\mathrm{d}z} u_L(z)\bigg|_I \quad \text{in the Couette and channel flow cases} \tag{2.4}$$

or

$$\mu_G \frac{\mathrm{d}}{\mathrm{d}r} u_G(r)\bigg|_I = \mu_L \frac{\mathrm{d}}{\mathrm{d}r} u_L(r)\bigg|_I \quad \text{in the pipe flow case.} \tag{2.5}$$

Here u_L and u_G, μ_L and μ_G are the velocities and dynamic viscosities of the liquid and the gas. The set of assumptions made so far is not complete. It remains to be determined what happens in the gas layer. In the context of the idealised flow conditions assumed here two different assumptions for the flow in the gas layer can be made. The first assumption is that the basic flow in the gas layer essentially shows the same behaviour as the flow in the liquid layer. This means in the Couette flow case that a flow with a constant (albeit higher) shear rate develops in the gas layer (Vinogradova 1999). In the pressure driven cases it would be assumed (as in the case of PCAF (Joseph *et al.* 1997)) that the same mean streamwise pressure gradient Π acts as in the liquid layer, $\Pi_G = \Pi_L$. Note that this has both in the shear and the pressure driven cases the consequence that a constant net mass flow rate is present in the gas layer, $\dot{m}_G > 0$. To maintain a constant mass flow rate there must be a source of gas at the inflow (here formally at $x = -\infty$, where x is the streamwise coordinate) and a gas sink at the outflow ($x = \infty$).

The alternative assumption is that the gas contained in the gas layer is trapped, i.e. there is no net mass flow through the gas layer, $\dot{m}_G = 0$. In this case the flow in the gas layer resembles the flow within a lid-driven cavity in the limit of zero aspect ratio (Bye 1966; Yang *et al.* 2002). For cases with flat walls a Couette-Poiseuille flow develops in the gas layer accompanied by a linear stress profile. The finite streamwise velocity in the upper part of the gas layer is accompanied by a reverse flow in the vicinity to the wall. In the pipe flow case a similar counter-current flow is present in the gas layer but it has a more complicated analytical description due to the cylindrical geometry (see below).

It has been demonstrated e.g. in the experiments of Elbing *et al.* (2008) that it is possible to create conditions as described in the first assumption, i.e. achieving an air layer with a net mass flow rate by constant injection of air upstream of the air layer. However, in the context of superhydrophobic surfaces no air is injected, and the goal is to achieve a trapped air layer covering the surface of an immersed object partially or entirely similar to a plastron encasing some aquatic insects when diving underwater (Thorpe & Crisp 1947; Shirtcliffe *et al.* 2006; Flynn & Bush 2008; Ditsche-Kuru *et al.* 2011). In the case of a sphere covered by a plastron an analytic solution can be found in the Stokes flow limit, and it can be shown that a flow with zero net mass flow rate develops in the gas layer encapsulating the sphere (McHale *et al.* 2011). Taking these

Name	flow type	cond. in gas layer	references
CTT1	Couette flow	$\frac{\mathrm{d}u_G}{\mathrm{d}z} = \text{const}$	Vinogradova (1999)
CTT2	Couette flow	$\dot{m}_G = 0$	
CHSYM1	Symmetric pressure-driven channel flow	$\Pi_G = \Pi_L$	Than *et al.* (1987)
CHSYM2	Symmetric pressure-driven channel flow	$\dot{m}_G = 0$	
CHONE1	One-sided pressure-driven channel flow	$\Pi_G = \Pi_L$	Joseph & Renardy (1992)
CHONE1	One-sided pressure-driven channel flow	$\dot{m}_G = 0$	
PIPE1	Pipe flow	$\Pi_G = \Pi_L$	Joseph *et al.* (1984)
PIPE2	Pipe flow	$\dot{m}_G = 0$	

TABLE 1. Overview over the configurations studied. $\Pi = \nabla p$ is the mean streamwise pressure gradient and $\dot{m}$ the mass flow rate.

considerations into account the alternative assumption (zero mass flow rate in the gas layer) is the applicable one in the context of typical superhydrophobic surfaces.

In this paper, solutions for the flow under the conventional assumptions and under the new zero-mass flow rate assumption are compared. An overview of the configurations studied is given in Table 1. References for configurations that have been studied previously are also listed in this table. First, the analytic solution for the velocity profiles will be given. Resulting key quantities for flow over superhydrophobic surfaces, such as the change in drag and the apparent slip length, will be compared in the following sections.

3. Results

3.1. *Velocity profiles*

The derivation of the streamwise velocity profiles under the conditions outlined in the previous section is a lengthy algebraic exercise and will not be shown here. The velocity profiles are given in Tables 2 and 3; $c_\mu = \mu_L/\mu_G$ indicates the viscosity contrast and d the relative gas layer thickness ($d = \delta/h$ or $d = \delta/R$) where h is the channel height (Couette and one-sided channel flow) or half-height (symmetric channel flow) and R is the pipe radius depending on the configuration studied. In the cases CTT1, CHSYM1, CHONE1 and PIPE1 the solutions have been previously derived (Joseph *et al.* 1984; Than *et al.* 1987; Joseph & Renardy 1992).

In the Couette flow cases the presence of the gas layer leads to a reduction of the shear rate in the liquid layer. If a constant shear rate is assumed in the gas layer (CTT1), a viscosity contrast $c_\mu > 1$ is sufficient to achieve this. If the mass flow rate in the gas layer is zero, the shear rate in the liquid layer is reduced only for $c_\mu > 4$, and an increase is observed for smaller viscosity contrasts.

In the pressure driven symmetric channel flow and pipe flow cases the gas layer results in a shift of the velocity profile in the liquid layer. If the pressure gradient in the gas layer is equal to the pressure gradient in the liquid layer, the profile in the gas layer takes the same form as if the whole channel or pipe was filled by gas. While in the cases CHSYM1 and PIPE1 the shift in the velocity profile is always positive for finite gas layer thickness and $c_\mu > 1$, a downwards shift of the velocity profile can occur in the CHSYM2 and PIPE2 cases for low viscosity contrasts.

Under the zero-mass flow rate condition a counter-current flow develops in the lower part of the gas layer close to the wall. The zero-crossing in the velocity profile occurs at a distance of $\frac{2}{3}\delta$ from the wall in the Couette and pressure driven channel flow cases. In

Case	velocity in liquid u_L
CTT1	$\frac{U_0}{1+(c_\mu-1)d}\left(\frac{z}{h}-1\right)+U_0$
CTT2	$\frac{U_0}{1+\frac{d}{4}(c_\mu-4)}\left(\frac{z}{h}-1\right)+U_0$
CHSYM1	$\frac{\Pi h^2}{2\mu_L}\left[\frac{z^2}{h^2}-1-(c_\mu-1)\,d(2-d)\right]$
CHSYM2	$\frac{\Pi h^2}{2\mu_L}\left[\frac{z^2}{h^2}-1-\frac{1}{2}(c_\mu-1)\,d(1-d)+\frac{1}{2}d(3-d)\right]$
CHONE1	$\frac{\Pi h^2}{2\mu_L}\left(\frac{z}{h}-1\right)\left[\frac{\frac{z}{h}\left[1+(c_\mu-1)d\right]+(c_\mu-1)d(1-d)}{1+(c_\mu-1)d}\right]$
CHONE2	$\frac{\Pi h^2}{2\mu_L}\left[\left(\frac{z^2}{h^2}-1\right)+\frac{4+2(c_\mu-2)d^2}{4+(c_\mu-4)d}\left(1-\frac{z}{h}\right)\right]$
PIPE1	$\frac{\Pi R^2}{4\mu_L}\left[\frac{r^2}{R^2}-1-(c_\mu-1)\,d(2-d)\right]$
PIPE2	$\frac{\Pi R^2}{4\mu_L}\left[\frac{r^2}{R^2}-(1-d)^2-c_\mu\frac{2d(2-d)(1-d)^2\left[(2-d)d+(2-2d+d^2)\ln(1-d)\right]}{d(4-14d+12d^2-3d^3)+4(1-d)^4\ln(1-d)}\right]$

TABLE 2. Velocity profiles in liquid u_L for a given upper wall velocity U_0 or mean streamwise pressure gradient Π.

the pipe flow case the location of the zero crossing is a function of the relative gas layer thickness d

$$r(u_G=0)=R\sqrt{\xi^{-1}\mathrm{W}_0\left(\xi\,e^{\xi}\right)}, \tag{3.1}$$

where W_0 is main branch of the Lambert W function (Corless *et al.* 1996) and

$$\xi=-\frac{2d(2-d)+4(1-d)^2\ln(1-d)}{d^2(2-d)^2}. \tag{3.2}$$

In the limit of small relative gas layer thickness, $d\to 0$, the radius of the zero crossing tends towards $r(u_G=0)=\left(1-\frac{2}{3}d\right)R$, i.e. the zero crossing occurs at a distance $\frac{2}{3}\delta$ from the wall corresponding to the solution for the channel flow cases. For very high relative gas layer thicknesses, $d\to 1$, the radius of the zero crossing approaches

$$r(u_G=0)=\frac{R}{\sqrt{-2(\mathrm{W}_0(-2/e^2))^{-1}}}\approx 0.4508R\quad\text{for } d\to 1. \tag{3.3}$$

Examples for velocity profiles are shown in figure 3 for $\delta/h=1/4$ and a viscosity contrast of $c_\mu=20$. In the pressure driven cases, the pressure gradient Π has been

case	velocity in gas u_G
CTT1	$\frac{U_0 c_\mu}{1+(c_\mu-1)d}\frac{z}{h}$
CTT2	$c_\mu \frac{U_0}{d[(c_\mu-4)d+4]}\frac{z}{h}\left(3\frac{z}{h}-2d\right)$
CHSYM1	$\frac{\Pi h^2}{2\mu_G}\left(\frac{z^2}{h^2}-1\right)$
CHSYM2	$\frac{3\Pi h^2}{4\mu_G}\frac{(1-d)}{d}\left[\left(-\frac{z^2}{h^2}+1\right)+\frac{2}{3}(3-d)\left(\frac{\lvert z\rvert}{h}-1\right)\right]$
CHONE1	$\frac{\Pi h^2}{2\mu_G}\frac{z}{h}\left[\frac{z}{h}-\frac{1+(c_\mu-1)d^2}{1+(c_\mu-1)d}\right]$
CHONE2	$\frac{\Pi h^2}{2\mu_G}\frac{3(1-d)^2}{d[4+(c_\mu-4)d]}\left(\frac{2}{3}d\frac{z}{h}-\frac{z^2}{h^2}\right)$
PIPE1	$\frac{\Pi R^2}{4\mu_G}\left(\frac{r^2}{R^2}-1\right)$
PIPE2	$\frac{\Pi R^2}{4\mu_G}\frac{2(1-d)^2[d(2-d)+2(1-d)^2\ln(1-d)]}{d(4-14d+12d^2-3d^3)+4(1-d)^4\ln(1-d)}\left[\frac{r^2}{R^2}-\frac{d^2(2-d)^2}{(2-d)d+2(1-d)^2\ln(1-d)}\ln\left(\frac{r}{R}\right)-1\right]$

TABLE 3. Velocity profiles in gas u_G for a given upper wall velocity U_0 or mean streamwise pressure gradient Π.

adjusted for each case so that a mass flow rate in the liquid phase equal to the mass flow rate in the corresponding reference case (no gas layer) results.

In the Couette flow case, the conventional condition for the flow in the gas layer, i.e. a constant shear rate, results in a much higher velocity in the liquid phase and a lower shear rate than in the case where a zero mass flow rate is assumed in the gas layer.

In the pressure driven cases the presence of the gas layer gives a much lower curvature (corresponding to a lower value of $-\Pi$) of the mean streamwise velocity profile in the liquid phase. If a zero mass flow rate is assumed in the gas layer the curvature is higher compared to the equal pressure gradient case. The largest differences in the velocity profile can be observed in the gas phase, where a strong counter-current flow is present in the lower part of the profile near the wall under the zero-mass flow rate assumption. For the one-sided channel flow the peak of the velocity profile always lies in the liquid domain if a zero mass flow rate is assumed for the gas layer, since the derivative of the profile u_G is positive near the interface. This condition does not apply in the corresponding equal pressure gradient case.

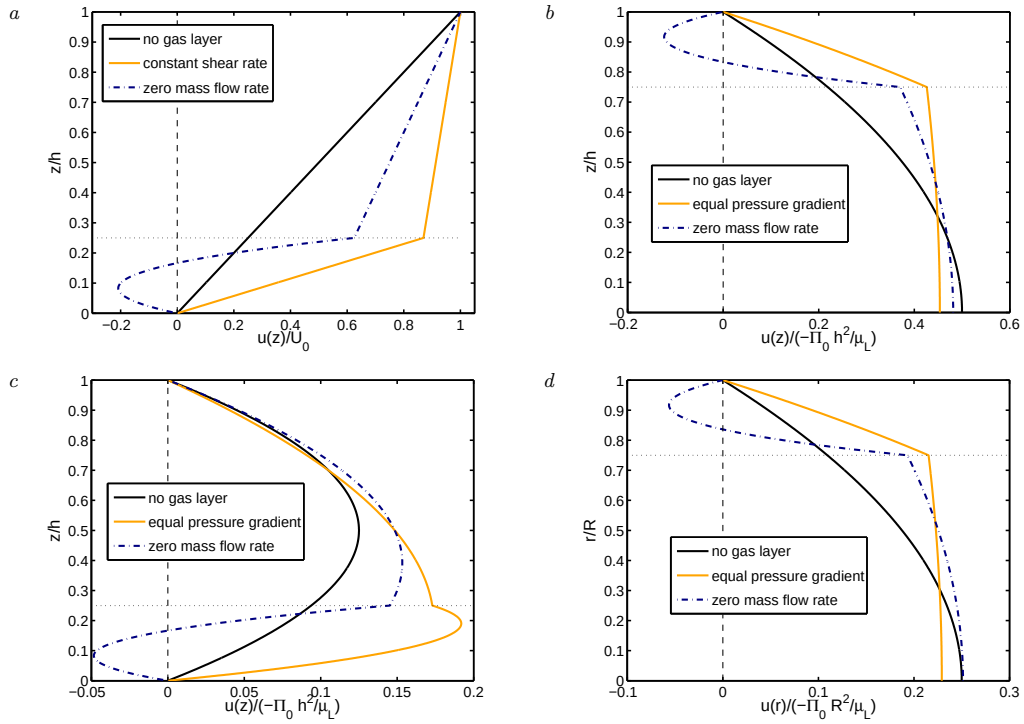

FIGURE 3. Mean streamwise velocity profile for a gas layer thickness of $\delta/h = 1/4$ and a viscosity contrast of $c_\mu = 20$. (a) Couette flow case; (b) symmetric channel flow case (only the upper half of channel is shown); (c) one-sided channel flow case; (d) pipe flow case. In the pressure driven cases the mean streamwise pressure gradients Π have been adjusted so that the same mass flow rates as in the respective no gas layer cases result. The thin horizontal dotted lines indicate the location of the gas-liquid interface.

3.2. *Change in drag*

In the context of fluid mechanics, the main motivation for the application of superhydrophobic surfaces is to reduce the drag. The change in drag is therefore the key quantity that needs to be considered. In the Couette flow cases the change in drag is based on the change in the shear rate at the upper wall $\dot{\gamma}_h = \frac{\mathrm{d}u}{\mathrm{d}z}\big|_{z=h}$

$$\Delta D_{\dot{\gamma}} = \frac{\dot{\gamma}_h - \dot{\gamma}_{h,0}}{\dot{\gamma}_{h,0}}, \tag{3.4}$$

where $\dot{\gamma}_{h,0}$ is the shear rate at the upper wall in the case of a vanishing gas layer. In the pressure driven cases the change in drag is defined based on the change on the mean streamwise pressure gradient $\frac{dp}{dx} = \Pi$ that needs to be applied to maintain a constant mass flow rate in the liquid phase

$$\Delta D_\Pi = \frac{\Pi - \Pi_0}{\Pi_0}. \tag{3.5}$$

Here Π_0 is the mean streamwise pressure gradient in the corresponding reference case without a gas layer. A positive ΔD corresponds to a drag increase whereas negative ΔD indicates drag reduction.

The expressions for the change in drag can be split into two parts,

$$\Delta D = L + B, \tag{3.6}$$

case	L	B
CTT1	$-\frac{(c_\mu-1)d}{(c_\mu-1)d+1}$	0
CTT2	$-\frac{(c_\mu-1)d}{(c_\mu-4)d+4}$	$\frac{3d}{(c_\mu-4)d+4}$
CHSYM1	$\frac{-3\left(c_\mu-1\right)(2-d)d}{3\left(c_\mu-1\right)d(2-d)+2+2d-d^2}$	$\frac{(3-d)d^2}{(1-d)\left[3\left(c_\mu-1\right)d(2-d)+2+2d-d^2\right]}$
CHSYM2	$\frac{-3\left(c_\mu-1\right)d}{3\left(c_\mu-1\right)d+(4-d)}$	$\frac{(3-d)^2d}{(1-d)^2\left[3\left(c_\mu-1\right)d+(4-d)\right]}$
CHONE1	$\frac{-\left(c_\mu-1\right)(3-9d+6d^2-d^3)d}{(1-d)^2\left[\left(c_\mu-1\right)d(4-d)+(1+2d)\right]}$	$\frac{d^2(3-2d)}{(1-d)^2\left[\left(c_\mu-1\right)d(4-d)+(1+2d)\right]}$
CHONE2	$\frac{-\left(c_\mu-1\right)(3-12d+12d^2-4d^3)d}{4(1-d)^3\left[1+d\left(c_\mu-1\right)\right]}$	$\frac{d(3-2d)^2}{4(1-d)^3\left[1+\left(c_\mu-1\right)d\right]}$
PIPE1	$\frac{-2\left(c_\mu-1\right)d(2-d)}{2\left(c_\mu-1\right)d(2-d)+1+2d-d^2}$	$\frac{d^2(2-d)^2}{(1-d)^2\left[2\left(c_\mu-1\right)d(2-d)+1+2d-d^2\right]}$
PIPE2	$\frac{4(c_\mu-1)(2-d)d\left[(2-d)d+(2-2d+d^2)\ln(1-d)\right]}{N}$	$\frac{(2-d)d}{(1-d)^4}\,\frac{(2-d)^3d^3}{N}$

where $N = 4(c_\mu - 1)d(2-d)\left[d(d-2) - (2-2d+d^2)\ln(1-d)\right] + (2-d)d(d^2-2d-2) - 4\ln(1-d)$

TABLE 4. Change in drag. The change in drag is split into a lubrication term L and a blockage term B.

the first term L is non-zero only for viscosity contrasts $c_\mu \neq 1$ and sums the effects due to lubrication. The second term B contains adverse effects of the gas layer and is greater than or equal to zero. In the pressure driven cases the blockage term is greater than zero, $B > 0$, for finite gas layer thicknesses, $\delta > 0$, and captures the drag increasing effects due to blockage of the channel or pipe caused by the reduction of the cross section due to the gas layer. In table 4 analytic relations for the change in drag are listed. The expressions in the denominator are always greater than or equal to zero for $0 \leq d \leq 1$ and $c_\mu \geq 1$.

In the Couette flow case no blockage (i.e. reduction of the mass flow rate due to the decreased cross section) exists due to the different definition for the change in drag. However there is an adverse blockage-like effect of the gas layer in the zero mass flow rate case (CTT2) for small viscosity contrasts giving a finite value for B. The change in drag, illustrated in figure 4, is always less than or equal to zero for $c_\mu \geq 1$ (CTT1) or $c_\mu \geq 4$ (CTT2). Even for $c_\mu \gg 4$ the change in drag is considerably smaller under the zero mass flow rate assumption for the gas layer compared to the constant shear rate case. In the limit of thin gas layers and high viscosity contrasts the ratio between the drag reduction for case CTT2 compared to case CTT1 tends to

$$\lim_{c_\mu \to \infty} \left(\lim_{d \to 0} \frac{\Delta D_{\mathrm{CTT2}}}{\Delta D_{\mathrm{CTT1}}} \right) = \lim_{c_\mu \to \infty} \left(\frac{c_\mu - 4}{4\,(c_\mu - 1)} \right) = \frac{1}{4}. \tag{3.7}$$

Hence, in the context of superhydrophobic surfaces, where the gas layer is usually quite thin and the viscosity contrast between liquid and gas is comparatively high, the drag reduction under the zero mass flow rate assumption is approximately 1/4 of the value under the constant shear rate conditions in the gas layer.

In the pressure driven channel and pipe flow cases the change in drag, shown in figure

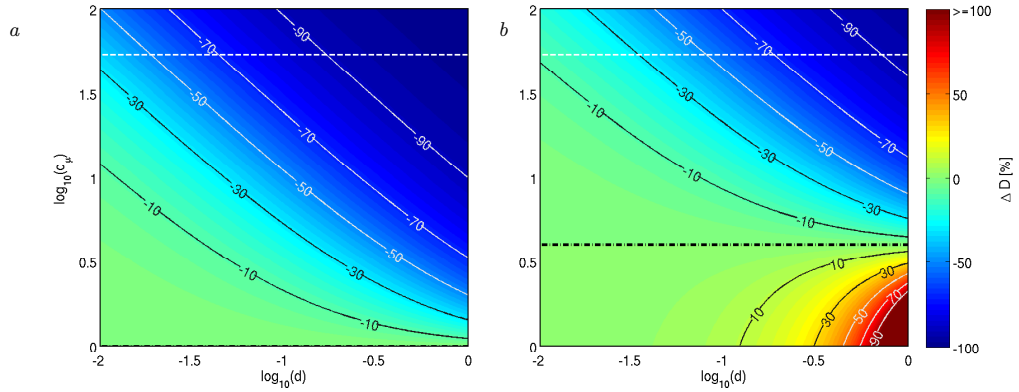

FIGURE 4. Change in drag $\Delta D_{\dot{\gamma}}$ for the Couette flow cases. (a) for CTT1: constant shear rate assumption. (b) for CTT2: zero mass flow rate assumption. The dashed white line indicates the case for the viscosity contrast between water and air. The dash-dotted black line shows the boundary between drag reduction and drag increase.

5, is more complicated since both the lubrication and the blockage term influence the change in drag. The lubrication term L is always negative for $c_\mu > 1$ in the symmetric channel flow and pipe flow cases, but can take both negative and positive values in the one-sided channel flow cases. For finite gas layer thicknesses the blockage term B is always positive (drag increasing), it decreases with increasing viscosity contrast and increases with the gas layer thickness. As in the Couette flow case, a minimum viscosity contrast of $c_\mu = 4$ needs to be exceeded to achieve drag reduction if a zero mass flow rate is assumed in the gas layer whereas drag reduction can be achieved for $c_\mu > 1$ in the equal pressure gradient case. Due to the blockage effects, the gas layer does not always have a drag reducing effect in the pressure-driven cases. For high gas layer thicknesses drag reduction can be achieved only for very high viscosity contrasts. In the one-sided channel flow case there is a maximum gas layer thickness beyond which the drag is always increased irrespective of the viscosity contrast; this (relative) gas layer thickness corresponds to the value of d for which the lubrication terms becomes zero, i.e. for

$$d_{\max}^{\mathrm{CHONE1}} = 2 - \cos(\pi/9) - \sqrt{3}\sin(\pi/9) \approx 0.468, \quad d_{\max}^{\mathrm{CHONE2}} = 1 - \frac{1}{2}2^{1/3} \approx 0.370. \quad (3.8)$$

The maximum gas layer thickness is significantly higher for the case with equal pressure gradient (CHONE1), since the lubrication effects of the gas layer are stronger. In the symmetric channel flow and pipe flow cases the lubrication term is always negative for $0 < \delta < h$ and thus there exists no maximum gas layer thickness $d_{\max} < 1$.

In the limit of thin gas layers, $d \to 0$, the ratio of the change in drag in the zero mass flow rate case compared to the corresponding equal pressure gradient case is appreciable. The limits derived for the Couette flow case, given in relation (3.7), also apply in the pressure driven case, i.e. the drag reduction under the zero mass flow rate assumption is less than or equal to 1/4 of the the drag reduction in the equal pressure gradient case.

3.3. *Optimum gas layer thickness*

As discussed above, in the pressure-driven channel and pipe flow cases the gas layer has two counteracting effects. Firstly, it lubricates the flow in the liquid layer and thus a smaller pressure gradient is sufficient to achieve a certain mass flow rate. Secondly, the gas layer occupies space in the channel or pipe and reduces the cross-section for the liquid flow which has adverse effects on the drag reduction. For very thin gas layers the first

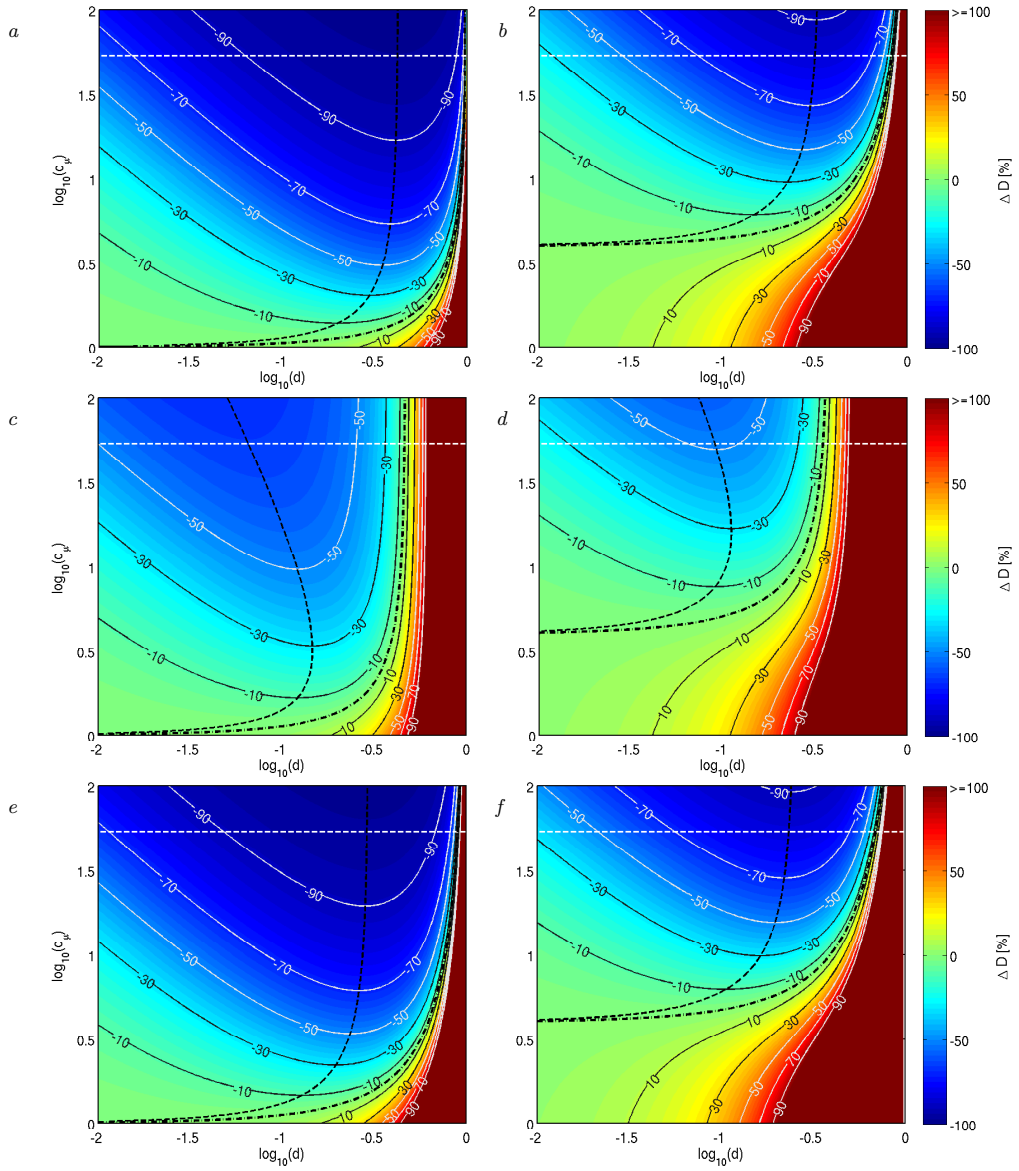

FIGURE 5. Change in drag ΔD_Π in the pressure driven channel and pipe flow cases. Left column: equal pressure gradient assumption. Right column: zero mass flow rate assumption. (a), (b): symmetric channel flow case; (c), (d): one-sided channel flow case; (e), (f): pipe flow case. The dashed white line indicates the case for the viscosity contrast between water and air. The dash-dotted black line shows the boundary between drag reduction and drag increase. The dashed black line indicates the optimum gas layer thickness.

effect dominates while for very thick gas layers the second effect is more important. Since the lubricating effect of the gas layer increases as a function of its thickness, there must be an optimum relative gas layer thickness d^{opt} between these two extremes.

The optimum gas layer thickness is found by minimising the change in drag for a given viscosity contrast. The resulting values are listed in Table 5 and the optimum gas layer thickness is indicated in Figure 5 by the dashed lines. The expressions for the

Case	$d^{\mathrm{opt}}(c_\mu)$	$d_\infty^{\mathrm{opt}} = \lim_{c_\mu \to \infty} d^{\mathrm{opt}}(c_\mu)$
CHSYM1	$1 - \sqrt{\frac{c_\mu}{3c_\mu - 2}}$	$1 - \sqrt{1/3} \approx 0.423$
CHSYM2	$\frac{c_\mu - 4}{3c_\mu - 4}$	$1/3$
CHONE1	$\frac{c_\mu(3c_\mu-1)(3\sin(\eta)-\sqrt{3}\cos(\eta))}{3(c_\mu-1)\sqrt{c_\mu(3c_\mu-1)}} + 1,$ where $\eta = \frac{1}{3}\arg(-9\sqrt{c_\mu} + 9c_\mu^{3/2} + \sqrt{3 + 54c_\mu - 81c_\mu^2})$	0
CHONE2	$\frac{4-3c_\mu+(c_\mu)^{3/2}}{4-5c_\mu+(c_\mu)^2}$	0
PIPE1	$1 - \sqrt{\frac{c_\mu}{2c_\mu - 1}}$	$1 - \frac{1}{\sqrt{2}} \approx 0.293$
PIPE2	approximate solution: $\frac{c_\mu - 4}{(d_\infty^{\mathrm{opt}})^{-1} c_\mu - 4}$	≈ 0.2479

TABLE 5. Optimum relative gas layer thickness d^{opt} as a function of the viscosity contrast c_μ for the pressure driven channel and pipe flow cases. d_∞^{opt} is the value of the optimum relative gas layer thickness in the limit of an infinite viscosity contrast.

optimum gas layer thickness given in Table 5 for the cases CHSYM1 and PIPE1 have been previously derived in the context of PCAF (Joseph *et al.* 1984; Than *et al.* 1987). In the PIPE2 case no analytic solution could be found. The optimum gas layer thickness shown in Figure 5 is a numerical approximation of the solution. A simple approximate expression for the optimum gas layer thickness is given in table 5 which is close to the numerical solution of the exact transcendent equation (see appendix A).

In the symmetric channel and pipe flow cases the optimum gas layer thickness approaches a constant finite value in the limit of high viscosity contrasts. Due to the cylindrical geometry, the optimum gas layer thickness is lower in the pipe flow case compared to the symmetric channel flow case. In the one-sided channel flow cases the optimum gas layer thickness is smaller than for the other two pressure driven configurations and tends towards zero for high viscosity contrasts. At a viscosity contrast of 50, i.e. approximately the contrast of water to air under standard conditions, the optimum gas layer thickness is significantly lower, too (see table 6).

The fact that the optimum gas layer thickness is quite high at typical viscosity contrasts appears to be discouraging since it is challenging to achieve gas layers of high thickness. However, the minimum of the change in drag is quite flat, especially in the symmetric channel flow and pipe flow cases (see example shown in figure 6), and thus considerably thinner gas layers are sufficient to achieve high drag reductions which are close to the optimum value (see example given in table 6).

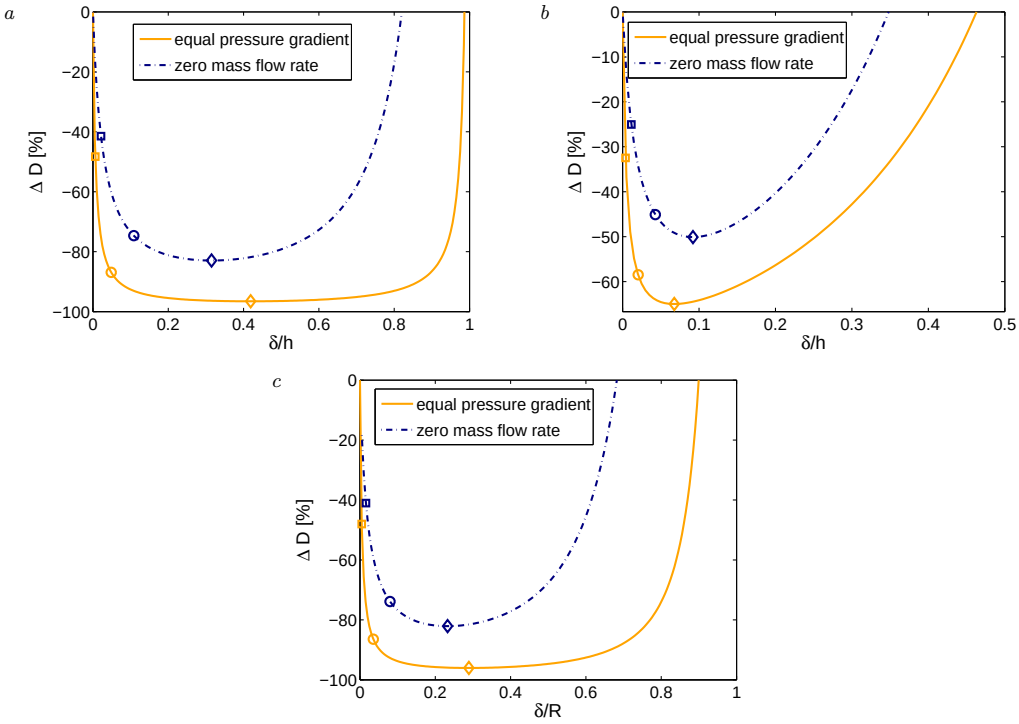

FIGURE 6. Change in drag as a function of the relative gas layer thickness δ/h for a viscosity contrast of $c_\mu = 50$. (a) symmetric channel flow case; (b) one-sided channel flow case; (c) pipe flow case. The diamonds show the optimum gas layer thickness / maximum drag reduction, whereas the circles and squares indicate the gas layer thicknesses needed to achieve 90% and 50% of the maximum drag reduction.

Case	$\Delta D_{\mathrm{opt}}[\%]$	d^{opt}	$d^{90\%}$	$d^{50\%}$
CHSYM1	−96.56	0.419	0.0487	0.00641
CHSYM2	−82.95	0.315	0.109	0.0215
CHONE1	−64.97	0.0677	0.0204	0.00395
CHONE2	−50.09	0.0921	0.0429	0.0115
PIPE1	−96.04	0.289	0.0356	0.00477
PIPE2	−82.08	0.233	0.0799	0.0159

TABLE 6. Values for the optimum change in drag ΔD_{opt}, optimum relative gas layer thickness d^{opt} and the relative gas layer thicknesses needed to achieve 90% and 50% of the optimum for a viscosity contrast of $c_\mu = 50$.

3.4. *Apparent slip length*

Macroscopically, the effect of a superhydrophobic surface is usually parametrised by a Navier slip length boundary condition (Vinogradova 1999; Lockerby *et al.* 2004; Min & Kim 2004; Rothstein 2010; Busse & Sandham 2012)

$$u_{\mathrm{slip}} = L_{\mathrm{slip}} \frac{\partial u}{\partial z}\bigg|_{\mathrm{wall}}, \tag{3.9}$$

where a finite slip velocity u_{slip} exists on the wall, which is proportional to the derivative of the velocity at the wall, and L_{slip} is the slip length. Different techniques are employed to

measure the slip length of a superhydrophobic surface experimentally (Maali & Bhushan 2012).

3.4.1. *Slip length based on velocity profile*

If the profile of the velocity can be measured, e.g. using μ-PIV measurements (Ou & Rothstein 2005; Joseph *et al.* 2006; Truesdell *et al.* 2006; Tsai *et al.* 2009), the slip length at the wall can be computed using relation (3.9) based on the wall velocity and the derivative of the velocity at the wall giving $L_{\mathrm{slip}}^{\mathrm{der}}$. Different approaches are taken with regards to the selection of the location of the wall. The first approach (Vinogradova 1999) is to use the bottom of the roughness supporting the gas layer as the location of the wall. This necessitates the extension of the velocity profile of the liquid phase $u_{\mathrm{L}}(z)$ to this position, which is straightforward in the case of the laminar flows studied here. The second approach is to use the top of the roughness supporting the gas layer, i.e. the liquid-gas interface, for the wall location in the computation the apparent slip length (Ou & Rothstein 2005; Tsai *et al.* 2009). In this case, an extension of the velocity profile is not necessary. However, the second approach gives misleadingly high values for the slip length. For example, most rough surfaces without any trapped gas layer would give a positive slip length according to this definition, because there usually is a positive mean streamwise velocity near the top of the roughness (a positive slip is then found for the fully wetted Wenzel state of a superhydrophobic surface). Another argument against the second approach is that in practice superhydrophobic coatings / foils would be applied as an additional layer onto a smooth surface. The superhydrophobic effect needs to be strong enough to overcome the penalty of the extra coating, e.g. the slightly decreased cross-section of a pipe or channel or the increased volume/circumference of a coated object (McHale *et al.* 2011; Gruncell *et al.* 2012*a*). Therefore – as far as the drag reducing properties of a superhydrophobic surface are concerned – the correct comparison is to compare the effect relative to a smooth, uncoated wall, and thus in the present model the bottom of the gas layer should be used as the wall location for the computation of the apparent slip length.

Expressions for the slip length based on the derivative (i.e. using the first definition for the wall location) are given in table 7. In the Couette flow cases, the slip length is a linear function of the gas layer thickness. If a zero mass flow rate is assumed in the gas layer, the apparent slip length is less than a quarter of the classical value (Vinogradova 1999) derived based on a constant shear rate in the gas layer. In the pressure driven cases, the slip length is a nonlinear function of the gas layer thickness. If an equal pressure gradient is assumed in the gas layer (CHSYM1, CHONE1, PIPE1), the slip length is always positive for $c_\mu > 1$. Under the zero mass flow rate assumption for the flow in the gas layer the slip length is negative for $c_\mu < 4$, and even for viscosity contrasts $c_\mu > 4$ the slip length is not always positive. In the limit of thin gas layers the slip length for the zero mass flow rate cases is always less than one quarter of the value for the equal pressure gradient cases. A positive slip length does not always correspond to a drag reduction in the pressure driven cases, since due to the blockage effects a positive slip length might not be high enough to overcome the losses due to a reduced diameter.

3.4.2. *Slip length based on mean flow quantities*

It is often not possible to measure the velocity profile and only mean flow quantities such as the change in the pressure drop or the mass flow rate can be obtained. In this case the slip length can be based on the change in the shear rate on the upper wall or the change in the pressure drop or mass flow rate (Ou *et al.* 2004; Ou & Rothstein 2005; Govardhan *et al.* 2009) by finding the analytic solution for a velocity profile that

Case	$L_{\mathrm{slip}}^{\mathrm{der}}$
CTT1	$(c_\mu - 1)d\,h$
CTT2	$\frac{1}{4}(c_\mu - 4)d\,h$
CHSYM1	$(c_\mu - 1)\left(1 - \frac{1}{2}d\right)dh$
CHSYM2	$\frac{1}{4}\left[(c_\mu - 1)(1-d) - (3-d)\right]d\,h$
CHONE1	$(c_\mu - 1)(1-d)\left[1 + (c_\mu - 1)d^2\right]^{-1} d\,h$
CHONE2	$\frac{1}{4}\left[(c_\mu - 4) - 2(c_\mu - 2)d\right]\left[1 + \frac{1}{2}d^2(c_\mu - 2)\right]^{-1} d\,h$
PIPE1	$\frac{1}{2}(c_\mu - 1)(2-d)\,d\,R$
PIPE2	$\frac{(2-d)\left[(2-d)d\left(2c_\mu(1-d)^2-2+6d-3d^2\right)+2(1-d)^2\left(c_\mu(2-2d+d^2)-2(1-d)^2\right)\ln(1-d)\right]}{2d(4-14d+12d^2-3d^3)+8(1-d)^4\ln(1-d)}d\,R$

TABLE 7. Apparent slip length based on derivative of velocity profile at the wall $L_{\mathrm{slip}}^{\mathrm{der}}$.

Case	L_{slip}^{Π}
CHSYM1	$\frac{1}{6}\left[(c_\mu - 1)\left(6 - 9d + 3d^2\right) - (3-d)\,d\right]d\,h$
CHSYM2	$\frac{1}{12}\left[3(c_\mu - 1)(1-d)^2 - (3-d)^2\right]d\,h$
CHONE1	$\frac{(c_\mu-1)\left(-d^3+6d^2-9d+3\right)-d(3-2d)}{3+d^2\left[(c_\mu-1)(3-d)^2-2d+3\right]}d\,h$
CHONE2	$\frac{1}{4}\frac{(c_\mu-1)\left(3-12d+12d^2-4d^3\right)-(3-2d)^2}{3+d^2\left[(c_\mu-1)\left(d^2-3d+3\right)-3+d\right]}d\,h$
PIPE1	$\frac{1}{4}(2-d)\left[2(c_\mu - 1)(1-d)^2 - d(2-d)\right]d\,R$
PIPE2	$\frac{(2-d)\left[4(c_\mu-1)(1-d)^4((2-d)d+(2-2d+d^2)\ln(1-d))+(2-d)^3d^3\right]}{4(d(4-14d+12d^2-3d^3)+4(1-d)^4\ln(1-d))}d\,R$

TABLE 8. Apparent slip length based on the pressure gradient / change in drag L_{slip}^{Π}.

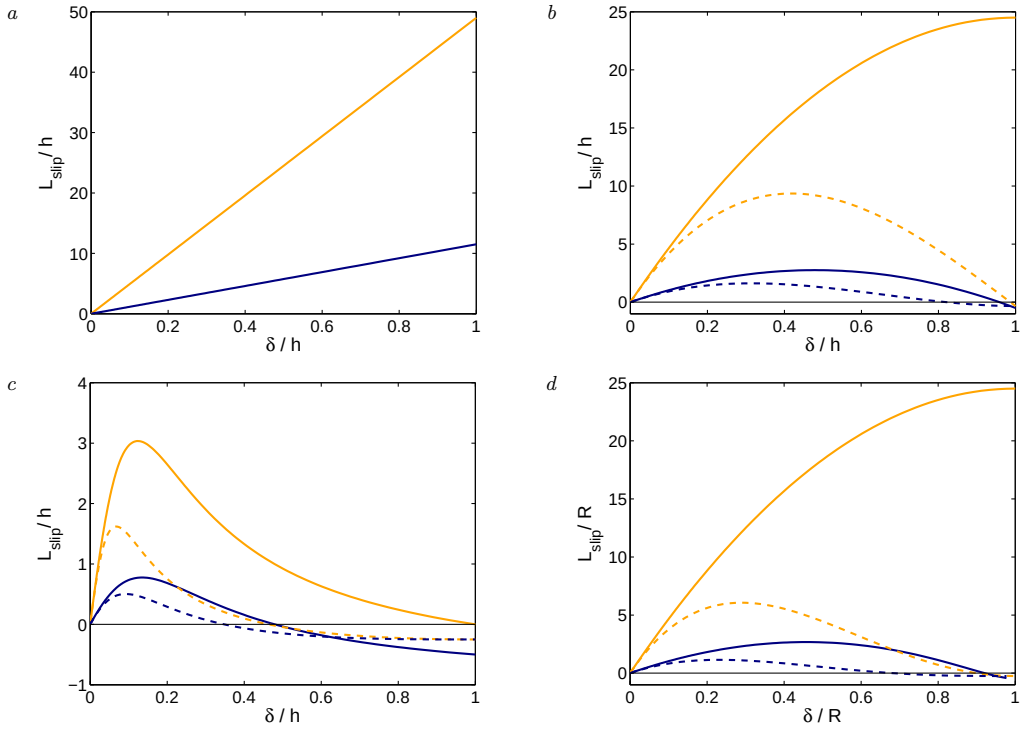

FIGURE 7. Slip length based vs gas layer thickness for a density contrast of $c_\mu = 50$. (a) Couette flow case; (b) symmetric channel flow case; (c) one-sided channel flow case; (d) pipe flow case. Light orange lines: constant shear (CTT1) or equal pressure gradient (CHSYM1, CHONE1, PIPE1); dark blue lines: zero mass flow rate in gas layer (CTT2, CHSYM2, CHONE2, PIPE2). Continuous lines: slip length based on derivative at wall; dashed lines: slip length based on mean flow quantities.

gives the same effect with the assumption of a a slip length boundary condition on the superhydrophobic walls. In the Couette flow case the resulting slip is equal to the slip length based on the local velocity profile at the wall, since the velocity profile is linear. In the pressure driven cases, where the velocity profile is a second order polynomial, the slip length based on the global flow quantities differs from the locally measured slip length discussed above (see Table 8). The slip length can be computed from the change in drag (3.5) using the following expressions

$$L^{\Pi}_{\mathrm{slip}} = \begin{cases} h\frac{\Pi_0-\Pi}{3\Pi} = -\frac{\Delta D\, h}{3(1+\Delta D)} & \text{for symmetric channel flow,} \\ h\frac{\Pi_0-\Pi}{4\Pi-\Pi_0} = -\frac{\Delta D\, h}{3+4\Delta D} & \text{for one-sided channel flow,} \\ R\frac{\Pi_0-\Pi}{4\Pi} = -\frac{\Delta D\, R}{4(1+\Delta D)} & \text{for pipe flow.} \end{cases} \tag{3.10}$$

As can be inferred from equation (3.10) the slip length based on the change in drag is always positive if there is a drag reduction ($\Delta D < 0$) and negative in the case of drag increase ($\Delta D > 0$). This also holds for the one-sided channel flow case, since the maximum possible drag reduction in this case is $\Delta D = -\frac{3}{4}$ for full slip on the lower wall (Ou & Rothstein 2005).

The two estimates for the slip length $L^{\mathrm{der}}_{\mathrm{slip}}$ and L^{Π}_{slip} are illustrated in figure 7. In the Couette flow case the slip length increases as a linear function of the viscosity contrast and the gas layer thickness. In the channel and pipe flow cases the estimate based on

the pressure drop is always lower than the estimate based on the derivative. However, for small gas layer thickness the two estimates are very close.

4. Conclusions

Analytic results have been derived for the flow over an idealised superhydrophobic surface. The results have been presented as a general function of the viscosity contrast and the relative gas layer thickness. They may also be applied in the context of superoleophobic and omniphobic surfaces. It was shown that the assumptions made for the flow in the gas layer strongly influence the resulting velocity profile, change in drag and apparent slip length. For a gas layer with constant shear rate (Couette flow case) or with a mean streamwise pressure gradient equal to the bulk phase (pressure driven channel and pipe flow cases) drag reduction can be achieved for a viscosity contrast in excess of unity. However, a minimum viscosity contrast in excess of four is a necessary requirement for drag reduction under the assumption that the gas is trapped (i.e. zero mass flow rate in the gas layer). Both the drag reduction and the apparent slip length are considerably lower under the trapped gas assumption. Therefore, conventional approaches, where the fact that the gas is trapped is not taken into account, significantly overpredict a possible drag reduction and apparent slip length.

For the pressure driven cases blockage has an adverse effect on a possible drag reduction. The optimum gas layer thickness for a given viscosity contrast therefore should not be exceeded. The optimum gas layer thickness is influenced relatively weakly by the conditions assumed for the gas layer. As the minimum of the change in drag or the maximum of the drag reduction is quite flat, much thinner gas layers are sufficient to get close to the maximum possible drag reduction for a given viscosity contrast. This is a promising result, since it is difficult to achieve superhydrophobic surfaces that can trap very thick air layers. A further observation is that a drag increase can correspond to a positive apparent slip length in the pressure driven cases if the slip length is based on the derivative of the velocity profile. Therefore positive slip is not a guarantor for drag reduction for pressure driven channel and pipe flow. In these cases the apparent slip length based on the mean flow quantities is probably a more reliable estimate.

The one-sided channel flow shows a distinctly different behaviour from the symmetric channel and the pipe flow cases. Here, the optimum gas layer thickness is much lower tending towards zero with increasing viscosity contrast. Furthermore, a maximum relative gas layer thickness d lower than unity exists in the one-sided channel flow cases, above which the drag is always increased. This maximum gas layer thickness is significantly larger for the equal pressure gradient case.

In this work a highly idealised superhydrophobic surface has been investigated. The surface structure supporting the air layer has been neglected and the air layer has been assumed to be of constant thickness. The current model may not represent the optimum superhydrophobic surface for all kinds of flows. In the case of turbulent flows a non-flat interface, e.g. with structures aligned with the streamwise direction in the manner of riblets (Garcia-Mayoral & Jimenez 2011), may given even higher benefits.

Constructing a superhydrophobic surface which allows a constant mass flow rate within the trapped medium, e.g. by blowing air through it similar to the air-layer drag reduction case in Elbing *et al.* (2008), has the potential of giving significantly higher drag reductions. However, at the same time, energy will have to be spent on achieving a continuous air flux, and in addition, the stability of the interface might be compromised.

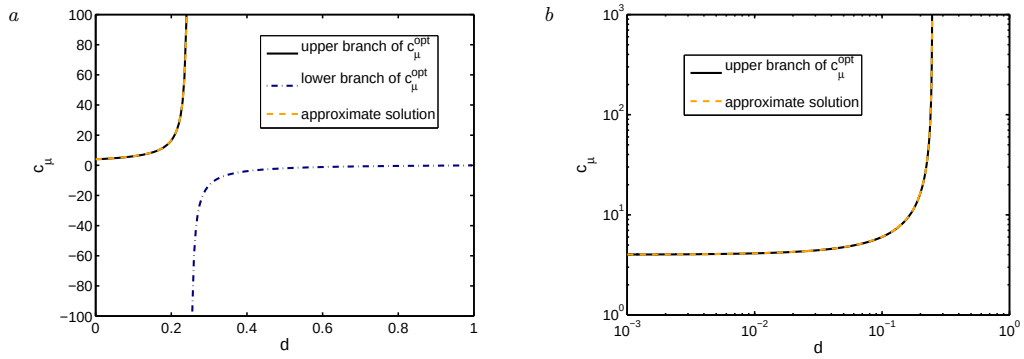

FIGURE 8. Exact and approximate solutions for optimum gas layer thickness for PIPE2 case. (a) on linear scales; (b) on logarithmic scales. Note that the lines for exact inverse solution (continuous black line) and the approximate solution (dashed light orange line) coincide almost perfectly.

Appendix A. Optimum gas layer thickness in case PIPE2

The optimum relative gas layer thickness in the case PIPE2 is the real solution for d between $[0, 1[$ of the following transcendent equation

$$\begin{aligned}(2-d)^2d^2\left[(c_\mu-1)(4-24d+64d^2-52d^3+13d^4)+4(2-d)^2d^2\right]+\\ 4(2-d)d\left[(c_\mu-1)(4-28d+86d^2-128d^3+102d^4-42d^5+7d^6)+\right.\\ \left.(2-d)^2d^2(2-2d+d^2)\right]\ln(1-d)+16(c_\mu-1)(1-d)^8(\ln(1-d))^2=0. \quad (A\,1)\end{aligned}$$

No analytic solution $d^{\mathrm{opt}}(c_\mu)$ for this equation could be found. However, it is possible to find the inverse function $c_\mu^{\mathrm{opt}}(d)$ of the solution

$$\begin{aligned}c_\mu^{\mathrm{opt}}(d)=\Big[d(4-14d+12d^2-3d^3)+4(1-d)^4\ln(1-d)\Big]^2\\ \Big[(2-d)^2d^2(4-24d+64d^2-52d^3+13d^4)+\\ 4d(8-60d+200d^2-342d^3+332d^4-186d^5+56d^6-7d^7)\ln(1-d)\\ +16(1-d)^8(\ln(1-d))^2\Big]^{-1}. \quad (A\,2)\end{aligned}$$

The function $c_\mu^{\mathrm{opt}}(d)$ is illustrated in figure 8. The upper branch corresponds to the optimum gas layer thickness; the lower branch gives negative values for the viscosity contrast and thus is not physical.

An approximate solution to equation (A 1) is given by

$$d^{\mathrm{opt}}=\frac{c_\mu-4}{(d_\infty^{\mathrm{opt}})^{-1}c_\mu-4} \quad (A\,3)$$

where d_∞^{opt} corresponds to the limit for the optimum gas layer thickness for an infinite viscosity contrast $\lim_{c_\mu\to\infty} d^{\mathrm{opt}}(c_\mu)\approx 0.24785$. As can be inferred from figure 8 the difference between the exact (inverse) solution and the approximate explicit solution is small.

REFERENCES

BHUSHAN, B. 2011 Biomimetics inspired surfaces for drag reduction and oleophobicity/philicity. *Beilstein Journal of Nanotechnology* **2**, 66–84.

Busse, A. & Sandham, N. D. 2012 Influence of an anisotropic slip-length boundary condition on turbulent channel flow. *Physics of Fluids* **24**, 055111.

Bye, J. A. T. 1966 Numerical solutions of the steady-state vorticity equation in rectangular basins. *Journal of Fluid Mechanics* **26**, 577–598.

Choi, C.-H., Westin, K. J. A. & Breuer, K. S. 2003 Apparent slip flows in hydrophilic and hydrophobic microchannels. *Physics of Fluids* **15** (10), 2897–2902.

Corless, R. M., Gonnet, G. H., Hare, D. E. G., Jeffrey, D. J. & Knuth, D. E. 1996 On the Lambert W function. *Advances in Computational Mathematics* **5**, 329–359.

Daniello, R. J., Waterhouse, N. E. & Rothstein, J. P. 2009 Drag reduction in turbulent flows over superhydrophobic surfaces. *Physics of Fluids* **21**, 085103.

Ditsche-Kuru, P., Schneider, E. S., Melskotte, J.-E., Brede, M., Leder, A. & Barthlott, W. 2011 Superhydrophobic surfaces of the water bug notonecta glauca: a model for friction reduction and air retention. *Beilstein Journal of Nanotechnology* **2**, 137–144.

Elbing, B. R., Winkel, E. S., Lay, K. A., Ceccio, S. L., Dowling, D. R. & Perlin, M. 2008 Bubble-induced skin-friction drag reduction and the abrupt transition to air-layer drag reduction. *Journal of Fluid Mechanics* **612**, 201–236.

Elboth, T., Reif, B. A. P., Andreassen, O. & Martell, M. B. 2012 Flow noise reduction from superhydrophobic surfaces. *Geophysics* **77**, P1–P10.

Flynn, M. R. & Bush, J. W. M. 2008 Underwater breathing: the mechanics of plastron respiration. *Journal of Fluid Mechanics* **608**, 275–296.

Garcia-Mayoral, Ricardo & Jimenez, Javier 2011 Drag reduction by riblets. *Philosophical Transactions of the Royal Society A* **369**, 1412.

Ghosh, S., Mandal, T.K., Das, G. & Das., P. K. 2009 Review of oil water core annular flow. *Renewable and Sustainable Energy Reviews* **13**, 1957–1965.

Gotge, S., Vorobieff, P., Truesdell, R., Mammoli, A. & van Swol, F. 2005 Effective slip on textured superhydrophobic surfaces. *Physics of Fluids* **17**, 051701.

Govardhan, R. N., Srinivas, F. S., Asthana, A. & Bobji, M. S. 2009 Time dependence of effective slip on textured hydrophobic surfaces. *Physics of Fluids* **21**, 052001.

Greidanus, A. J., Delfos, R. & Westerweel, J 2011 Drag reduction by surface treatment in turbulent Taylor-Couette flow. *J. Phys. Conf. Ser.* **318**, 082016.

Gruncell, B. R. K., Sandham, N. D. & McHale, G. 2012*a* Simulations of laminar flow past a superhydrophobic sphere with drag reduction and separation delay. *Physics of Fluids* **25**, 043601.

Gruncell, B. R. K., Sandham, N. D. & Prince, M. P. 2012*b* Experimental and numerical investigation of the drag on superhydrophobic surfaces. In *Proceedings of the 9th International ERCOFTAC Symposium on Engineering Turbulence Modelling and Measurements*.

Joseph, D. D., Bai, R., Chen, K. P. & Renardy, Y. Y. 1997 Core-annular flows. *Annual Review of Fluid Mechanics* **29**, 65–90.

Joseph, D. D., Nguyen, K. & Beavers, G. S. 1984 Non-uniqueness and stability of the configuration of flow of immiscible fluids with different viscosities. *Journal of Fluid Mechanics* **141**, 319–345.

Joseph, D. D. & Renardy, Y. Y. 1992 *Fundamentals of Two-Fluid Dynamics*. Springer-Verlag.

Joseph, P., Cottin-Bizonne, C., Benoît, J.-M., Ybert, C., Journet, C., Tabeling, P. & Bocquet, L. 2006 Slippage of water past superhydrophobic carbon nanotube forests in microchannels. *Physical Review Letters* **97**, 156104.

Landau, L. D. & Lifshitz, E. M. 1959 *Fluid Mechanics*. Pergamon Press.

Leidenfrost, J. G. 1966 On fixation of water in diverse fire. *International Journal of Heat and Mass Transfer* **9**, 1153.

Lockerby, D. A., Reese, J. M., Emerson, D. R. & Barber, R. W. 2004 Velocity boundary condition at solid walls in rarefied gas calculations. *Physical Review E* **70**, 017303.

Looman, M. D. 1916 US Patent No. 1,192,438.

Maali, A. & Bhushan, B. 2012 Measurement of slip length on superhydrophobic surfaces. *Proc. R. Soc. A* **370**, 2304–2320.

McHale, G., Flynn, M. R. & Newton, M.I. 2011 Plastron induced drag reduction and increased slip on a superhydrophobic sphere. *Soft Matter* **7** (21), 10100–10107.

McHale, G., Newton, M. I. & Shirtcliffe, N. J. 2010 Immersed superhydrophobic surfaces: Gas exchange, slip and drag reduction properties. *Soft Matter* **6**, 714–719.

McHale, G., Shirtcliffe, N. J., Evans, C. R. & Newton, M. I. 2009 Terminal velocity and drag reduction measurements on superhydrophobic spheres. *Applied Physics Letters* **94**, 064104.

Min, T. & Kim, J. 2004 Effects of hydrophobic surface on skin-friction drag. *Physics of Fluids* **16** (7), L55–58.

Muralidhar, P., Ferrer, N., Daniello, R. & Rothstein, J. P. 2011 Influence of slip on the flow past superhydrophobic circular cylinders. *Journal of Fluid Mechanics* **680**, 459–476.

Neto, C., Evans, D. R., Bonaccurso, E., Butt, H.-J. & Craig, V. S. J. 2005 Boundary slip in Newtonian liquids: a review of experimental studies. *Reports on Progress in Physics* **68**, 2859–2897.

Ou, J., Perot, B. & Rothstein, J. P. 2004 Laminar drag reduction in microchannels using ultrahydrophobic surfaces. *Physics of Fluids* **16**, 4635.

Ou, J. & Rothstein, J. P. 2005 Direct velocity measurements of the flow past drag-reducing ultrahydrophobic surfaces. *Physics of Fluids* **17**, 103606.

Quéré 2008 Wetting and roughness. *Annual Review of Materials Research* **42**, 89–109.

Rothstein, J. P. 2010 Slip on superhydrophobic surfaces. *Annual Review of Fluid Mechanics* **42**, 89–109.

Sadhal, S. S., Ayyaswamy, P. S. & Chung, J. N. 1996 *Transport Phenomena with Drops and Bubbles*. Springer-Verlag.

Shirtcliffe, N. J., McHale, G., Newton, M. I., Perry, C. C. & Pyatt, F. B. 2006 Plastron properties of a superhydrophobic surface. *Applied Physics Letters* **89**, 104106.

Than, P. T., Rosso, F. & Joseph, D. D. 1987 Instability of Poiseuille flow of two immiscible liquids with different viscosities in a channel. *Int. J. Engng Sci.* **25**, 189–204.

Thorpe, W. H. & Crisp, D. J. 1947 Plastron respiration in the Coleoptera. *Journal of Experimental Biology* **26**, 219–260.

Truesdell, R., Mammoli, A., Vorobieff, P., van Swol, F. & Brinker, C. J. 2006 Drag reduction on a patterned superhydrophobic surface. *Physical Review Letters* **97**, 044504.

Tsai, P., Peters, A. M., Pirat, Ch., Wessling, M., Lammertink, R. G. H. & Lohse, D. 2009 Quantifying effective slip length over micropatterned hydrophobic surfaces. *Physics of Fluids* **21**, 112002.

Tuteja, A., Choi, W., Ma, M., Mabry, J. M., Mazzella, S. A., Rutledge, G. C., McKinley, G. H. & Cohen, R. E. 2007 Designing superoleophobic surfaces. *Science* **318**, 1618.

Tuteja, A., Choi, W., Mabry, J. M., McKinley, G. H. & Cohen, R. E. 2008 Robust omniphobic surfaces. *PNAS* **105**, 18200–18205.

Vakareslki, I., Marston, J., Chan, D. & Thoroddsen, S. 2011 Drag reduction by Leidenfrost vapor layers. *Physical Review Letters* **106**.

Vinogradova, O. I. 1999 Slippage of water over hydrophobic surfaces. *International Journal of Mineral Processing* **56**, 31–60.

Vinogradova, O. I. & Dubov, A. L. 2012 Superhydrophobic textures for microfluidics. *Mendeleev Communications* **22** (5), 229–236.

Voronov, R. S., Papavassiliou, D. V. & Lee, L. L. 2008 Review of fluid slip over superhydrophobic surfaces and its dependence on the contact angle. *Industrial & Engineering Chemistry Research* **47**, 2455–2477.

Wong, T.-S., Tang, S. K. Y., Smythe, E. J., Hatton, B. D., Grinthal, A. & Aizenberg, J. 2011 Bioinspired self-repairing slippery surfaces with pressure-stable omniphobicity. *Nature* **477**, 443–447.

Yang, Y., Straatman, A. G., Martinuzzi, R. J. & Yanful, E. K. 2002 A study of laminar flow in low aspect ratio lid-driven cavities. *Canadian Journal of Civil Engineering* **29**, 436–447.